Spin-resolved Andreev levels and parity crossings in hybrid superconductor–semiconductor nanostructures

Spin-resolved Andreev levels and parity crossings in hybrid superconductor-semiconductor nanostructures

Eduardo J. H. Lee[1], Xiaocheng Jiang[2], Manuel Houzet[1], Ramón Aguado[3], Charles M. Lieber[2], and Silvano De Franceschi[1*]

[1]*SPSMS, CEA-INAC/UJF-Grenoble 1, 17 rue des Martyrs, 38054 Grenoble Cedex 9, France*
[2]*Harvard University, Department of Chemistry and Chemical Biology, Cambridge, MA, 02138, USA and*
[3]*Instituto de Ciencia de Materiales de Madrid (ICMM),*
Consejo Superior de Investigaciones Científicas (CSIC),
Sor Juana Inés de la Cruz 3, 28049 Madrid, Spain
(Dated: October 30, 2013)

The physics and operating principles of hybrid superconductor-semiconductor devices rest ultimately on the magnetic properties of their elementary sub-gap excitations, usually called Andreev levels. Here we report a direct measurement of the Zeeman effect on the Andreev levels of a semiconductor quantum dot with large electron g-factors, strongly coupled to a conventional superconductor with large critical magnetic field. This material combination allows spin degeneracy to be lifted without destroying superconductivity. We show that a spin-split Andreev level crossing the Fermi energy results in a quantum phase transition to a spin-polarized state, implying a change in the fermionic parity of the system. This crossing manifests itself as zero-bias conductance anomaly at finite magnetic field whose properties resemble those expected for Majorana modes in a topological superconductor. While this resemblance is understood without evoking topological superconductivity, the observed parity transitions could be regarded as precursors of Majorana modes in the long-wire limit.

When a normal-type (N) conductor is connected to a superconductor (S), superconducting order can leak into it giving rise to pairing correlations and an induced superconducting gap. This phenomenon, known as the superconducting proximity effect, is expected also when the N conductor consists of a nano-scale semiconductor whose electronic states have a reduced dimensionality and can be tuned by means of electric or magnetic fields. This hybrid combination of superconductors and low-dimensional semiconductors offers a versatile ground for novel device concepts [1]. Some examples include sources of spin-entangled electrons [2–4], nano-scale superconducting magnetometers [5], or recently proposed qubits based on topologically protected Majorana fermions [6–8]. Such concepts, which form an emerging domain between superconducting electronics and spintronics, rest on a rich and largely unexplored physics involving both superconductivity and spin-related effects [5, 9–12]. Here we address this subject by considering the lowest dimensional limit where the N conductor behaves as a small quantum dot (QD) with a discrete electronic spectrum. In this case, the superconducting proximity effect competes with the Coulomb blockade phenomenon, which follows from the electrostatic repulsion among the electrons of the QD [13]. While superconductivity priviliges the tunneling of electron pairs with opposite spin, thereby favoring QD states with even numbers of electrons and zero total spin (i.e. spin singlets), the local Coulomb repulsion enforces a one-by-one filling of the QD, thereby stabilizing not only even but also odd electron numbers.

In order to analyse this competition, let us consider the elementary case of a QD with a single, spin-degenerate orbital level. When the dot occupation is tuned to one electron, two ground states (GSs) are possible: a spin-doublet $(S = 1/2)$, $|D\rangle = |\uparrow\rangle, |\downarrow\rangle$, or a spin-singlet $(S = 0)$, $|S\rangle$, whose nature has two limiting cases. In the large superconducting gap limit $(\Delta \to \infty)$, the singlet is superconducting-like, $|S\rangle = -v^*|\uparrow\downarrow\rangle + u|0\rangle$, corresponding to a Bogoliubov-type superposition of the empty-state, $|0\rangle$, and the two-electron state, $|\uparrow\downarrow\rangle$. By contrast, in the strong coupling limit, where the QD-S tunnel coupling, Γ_S, is much larger than Δ, the singlet state is Kondo-like, resulting from the screening of the local QD magnetic moment by quasiparticles in S. Even though the precise boundary between the superconducting-like and Kondo-like singlet states is not well-defined [14], one can clearly identify changes in the GS parity, namely whether the GS is a singlet (fermionic even parity) or a doublet (fermionic odd parity), as we show here. The competition between the singlet and doublet states is governed by different energy scales: Δ, Γ_S, the charging energy, U, and the energy ϵ_0 of the QD level relative to the Fermi energy of the S electrode (see Fig. 1a) [14–23]. Previous works addressing this competition have focused either on Josephson supercurrents in S-QD-S devices [11, 24] or on the sub-gap structure in S-QD-S or N-QD-S geometries [25–33]. Although the QD-S GS could be inferred in some of the above studies, a true experimental demonstration of the GS parity requires its magnetic properties to be probed.

Here we report a tunnel spectroscopy experiment probing the magnetic properties of a QD-S system. With the aid of suitably large magnetic fields, we lift the degeneracy of the spinful states (i.e., $|D\rangle$) and measure the corresponding effect on the lowest-energy, sub-gap excitations of the system (i.e., $|D\rangle \leftrightarrow |S\rangle$ transitions). This
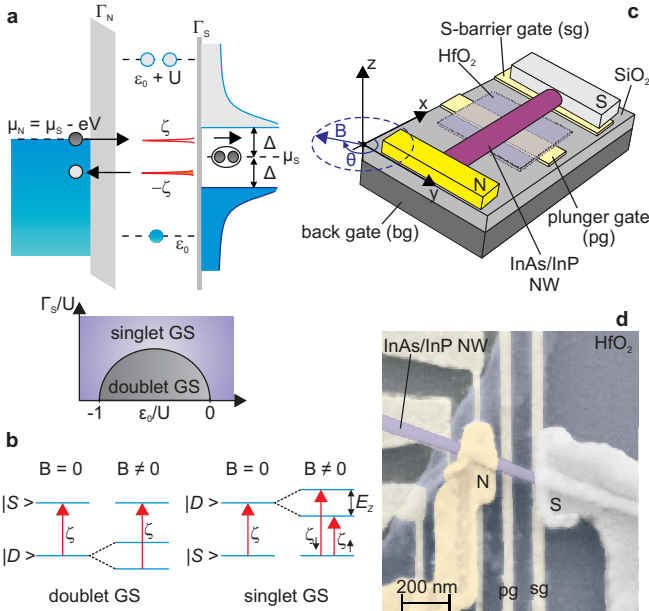
FIG. 1. **Andreev levels in a hybrid N-QD-S system and device description.** (a) (Upper panel) Schematics of a N-QD-S device with asymmetric tunnel couplings to the normal metal (Au) and superconductor (V) leads, Γ_N and Γ_S, respectively. Δ is the superconducting gap, U is the charging energy, μ_i is the chemical potential of the i lead, and ϵ_0 is the QD energy level relative to μ_S (in the $\Gamma_S \to 0$ limit, the QD has 0, 1 or 2 electrons for $\epsilon_0 > 0$, $-U < \epsilon_0 < 0$, $\epsilon_0 < -U$, respectively). The sub-gap peaks located at $\pm\zeta$ represent the Andreev levels. In tunnel spectroscopy measurements the alignment of μ_N to an Andreev level yields a peak in the differential conductance. This process involves an Andreev reflection at the QD-S interface, transporting a Cooper pair to the S lead and reflecting a hole to the N contact. (Lower panel) Qualitative phase diagram [16–19, 21] depicting the stability of the magnetic doublet ($|D\rangle = |\uparrow\rangle, |\downarrow\rangle$) versus that of the spin-singlet ($|S\rangle$). (b) Low-energy excitations of the QD-S system and their expected evolution in a magnetic field, B. Doublet GS case (left): $|\uparrow\rangle$ is stabilized by B and Andreev levels related to the transition $|\uparrow\rangle \to |S\rangle$ are observed. Singlet GS case (right): at finite B, the excited spin-split states $|\uparrow\rangle$ and $|\downarrow\rangle$ give rise to distinct Andreev levels with energy $\zeta_\uparrow$ and $\zeta_\downarrow$, respectively. $E_Z = |g|\mu_B B$ is the Zeeman energy, where $|g|$ is the g-factor and μ_B is the Bohr magneton. (c) Device schematic. The N and S leads were made of Ti(2.5 nm)/Au (50 nm) and Ti(2.5 nm)/V (45 nm)/Al (5 nm), respectively. The QD system is tuned by means of three gates: a plunger gate (pg), a barrier gate (sg) close to the S contact, and a back gate (bg). B is applied in the (x,y) device plane (x being parallel to the NW). (d) Scanning electron micrograph of a N-QD-S device.

experiment was carried out on a N-QD-S system, where the N contact is used as a weakly coupled tunnel probe. In this geometry, a direct spectroscopy of the density of states (DOS) in the QD-S system is obtained through a measurement of the differential conductance, dI/dV, as a function of the voltage difference, V, between N and S. In such a measurement, an electrical current measured for $|V| < \Delta/e$ is carried by so-called Andreev reflection

processes, each of which involves two single-electron transitions in the QD. For example, an electron entering the QD from N induces a single-electron transition from the QD GS, i.e. $|D\rangle$ or $|S\rangle$, to the first excited state (ES), i.e. $|S\rangle$ or $|D\rangle$, respectively. The ES relaxes back to the GS through the emission of an electron pair into the superconducting condensate of S and a second single-electron transition corresponding to the injection of another electron from N (the latter process is usually seen as the retroreflection of a hole into the Fermi sea of N). The just described transport cycle yields a dI/dV resonance, i.e. an Andreev level, at $eV = \zeta$, where ζ is the energy difference between ES and the GS, i.e. between $|D\rangle$ or $|S\rangle$, or vice-versa (see Fig. 1a). The reverse cycle, which involves the same excitations, occurs at $eV = -\zeta$, yielding a second Andreev level symmetrically positioned below the Fermi level.

In a magnetic field, the spin doublet splits due to the Zeeman effect. Remarkably, since Andreev levels are associated with low-energy transitions between states with different parity, a corresponding splitting of the Andreev levels is expected only for a spin-singlet GS (Fig. 1b, right). In the case of a spin-doublet GS, the spin-flip transition does not generate any measurable sub-gap resonance, and the Zeeman splitting of $|D\rangle$ results simply in an increase of ζ (Fig. 1b, left). The main goal of this work is to reveal the Zeeman effect on the Andreev levels of a QD-S system and to investigate its experimental signatures as a function of the relevant energy scales and the corresponding GS properties.

We used devices based on single InAs/InP core/shell nanowires (NWs), where vanadium (gold) was used for the S (N) contact [34]. A device schematic and a representative image are shown in Figs. 1c and 1d, respectively. The fabricated vanadium electrodes showed $\Delta = 0.55$ meV and an in-plane critical magnetic field $B_c^x \approx 2$ T ($x \parallel$ NW axis). The QD is naturally formed in the NW section between the S and N contacts. We find typical U values of a few meV (i.e., $U/\Delta \approx 3 - 10$). The QD properties are controlled by means of two bottom electrodes crossing the NW, labeled as plunger gate and S-barrier gate, and a back gate provided by the conducting Si substrate. To achieve the asymmetry condition $\Gamma_S \gg \Gamma_N$ ($\Gamma_S/\Gamma_N \approx 100$), the S-barrier gate was positively biased at $V_{sg} = 2$ V. We used the plunger gate voltage V_{pg} to vary the charge on the QD, and the back-gate voltage V_{bg} to finely tune the tunnel coupling. Transport measurements were performed in a dilution refrigerator with a base temperature of 15 mK.

Figure 2a shows a series of $dI/dV(V_{pg}, V)$ measurements for three different Γ_S. The top row refers to the weakest Γ_S. In this case, the spanned V_{pg} range corresponds to a horizontal path in the phase diagram that goes through the doublet GS region (see right diagram). Let us first consider the leftmost plot taken at magnetic field $B = 0$. On the left and right sides of this plot, the QD lies deep inside the singlet GS regime. Here the doublet ES approaches the superconducting gap edge, yielding an Andreev-level energy $\zeta \approx \Delta$. By moving to-
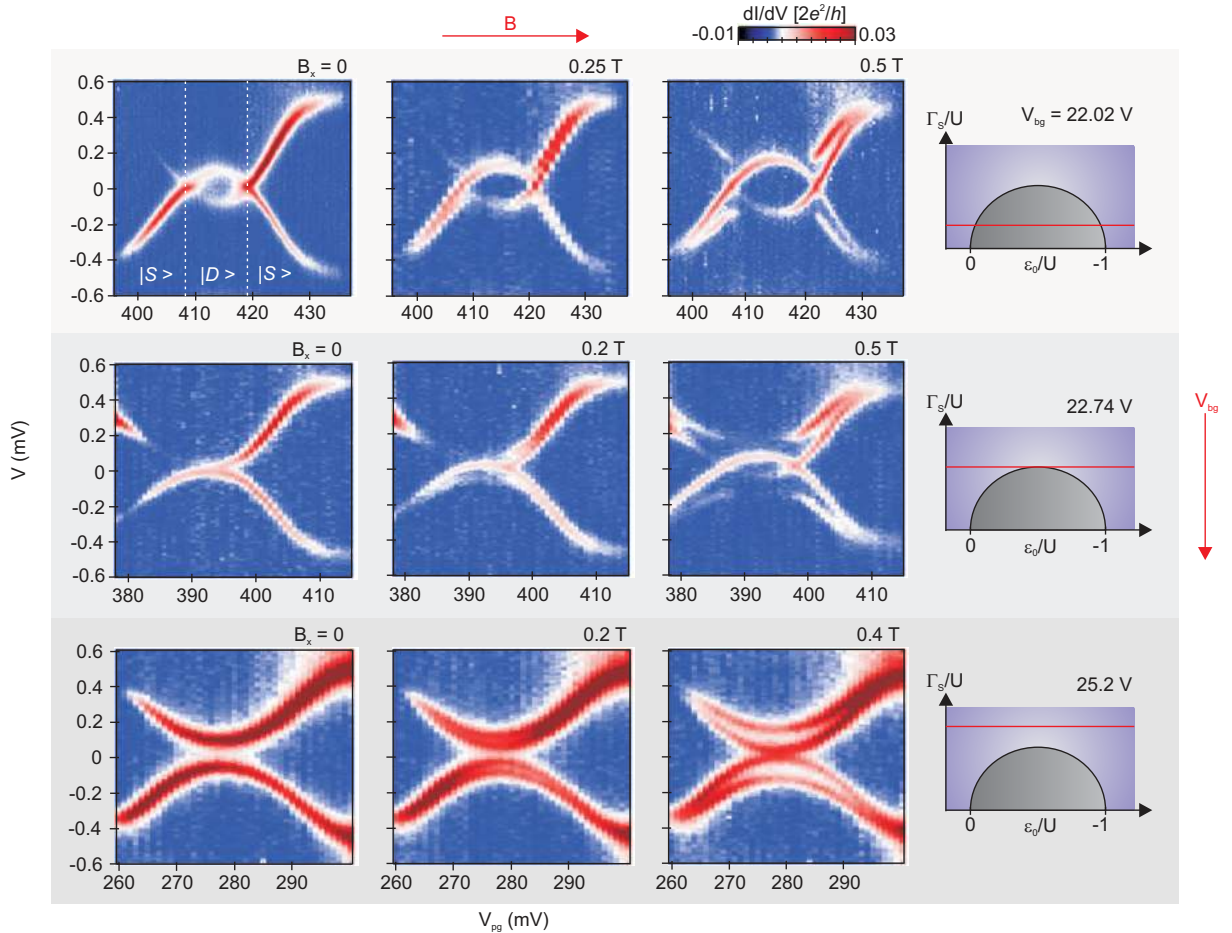
FIG. 2. **Andreev levels in different coupling regimes and their magnetic-field dependence.** (a) Experimental plots of dI/dV vs. (V_{pg}, V) for different QD-S couplings, Γ_S (increasing from top to bottom), and different B values (increasing from left to right). Top-left panel: along the V_{pg} range, the system GS changes from singlet ($|S\rangle$) to doublet ($|D\rangle$) and back to singlet, following the red trajectory in the qualitative diagram on the right side of the same row. We find that increasing V_{bg} results in larger Γ_S, thereby leading to an upward shift in the phase diagram. Eventually, the red trajectory is pushed into the singlet region (mid and bottom diagrams). Experimentally, this results in the disappearance of the doublet GS loop structure, as shown in the mid-left and bottom-left panels. The middle and right columns show the B-evolution of the Andreev levels in the three coupling regimes. For relatively weak coupling (top row), the Andreev levels for a singlet GS split due to the Zeeman effect, whereas those for a doublet GS simply move apart. At intermediate coupling (middle row), B induces a quantum-phase transition from a singlet to a spin-polarized GS, as denoted by the appearance of a loop structure (right panel). At the largest coupling (bottom row), the Zeeman splitting of the Andreev levels is clearly visible all over the V_{pg} range. The splitting is gate-dependent with a maximum in the central region.

wards the central region, the two sub-gap resonances approach each other and cross at the singlet-doublet phase boundaries, where $\zeta = 0$. In the doublet GS regime between the two crossings, the sub-gap resonances form a loop structure with ζ maximal at the electron-hole symmetry point. Increasing Γ_S corresponds to an upward shift in the phase diagram. The middle row in Fig. 2a refers to the case where Γ_S is just large enough to stabilize the singlet GS over the full V_{pg} range (see right diagram). At $B = 0$, the Andreev levels approach the Fermi level without crossing it. A further increase in Γ_S leads to a robust stabilization of the singlet GS (bottom row). At zero-field, the sub-gap resonances remain distant from each other coming to a minimal separation at the electron-hole symmetry point ($\epsilon_0 = -U/2$).

We now turn to the effect of B on the Andreev levels (middle and right columns in Fig. 2a). Starting from the weak coupling case (top row), a field-induced splitting of the sub-gap resonances appears, yet only in correspondence of a singlet GS. This is due to the fact that these resonances involve excitations between states of different parity. For a singlet GS, the spin degeneracy of the doublet ES is lifted by the Zeeman effect resulting in two distinct excitations (see Fig. 1b). By contrast, for a doublet GS, no sub-gap resonance stems from the $|\uparrow\rangle \rightarrow |\downarrow\rangle$ excitation, because these two states have the same (odd) number of electrons. The energy of the only visible Andreev level, associated with the $|\uparrow\rangle \rightarrow |S\rangle$ transition, increases with B. The formation of a loop structure in the rightmost panel of the middle row shows
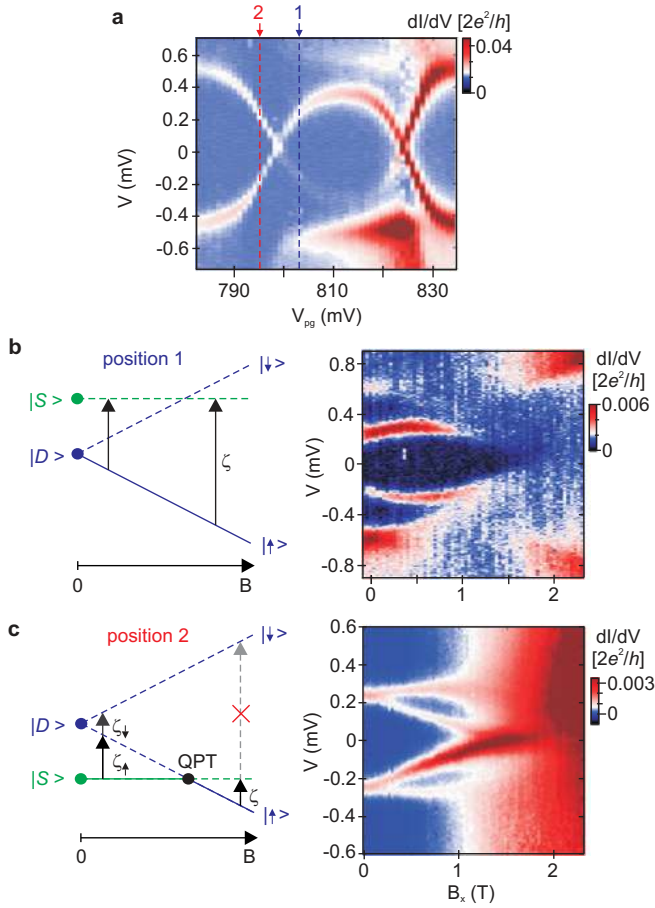
FIG. 3. **Magnetic-field evolution of the Andreev levels at fixed gate voltage and the level repulsion effect.** (a) $dI/dV(V_{pg}, V)$ measurement at $B = 0$ corresponding to a singlet-doublet-singlet sweep.(b) Left panel: Qualitative B-evolution of the low-energy states of a QD-S system as expected for a doublet GS. Right panel: Corresponding experimental data measured at position 1 in (a). ζ increases linearly with B until it approaches the edge of the superconducting gap. The levels then move towards zero following the B suppression of Δ. (c) same as (b), but for singlet GS. The experimental plot in the middle panel was taken at position 2 in (a). It shows an asymmetric splitting of the $\zeta_\uparrow$ and $\zeta_\downarrow$ peaks. The weak B dependence of $\zeta_\downarrow$ is due to the level repulsion between $|\downarrow\rangle$ and the continuum of quasiparticle states above Δ.

that a quantum phase transition (QPT) from a singlet to a spin-polarized GS can be induced by B when the starting ζ is sufficiently small. Importantly, this QPT is indicative of a change in the fermion parity of the ground state. In the bottom row, Zeeman-split Andreev levels can be seen all over the spanned V_{pg} range. At $B_x = 0.4$ T, the inner levels overlap at the Fermi level, indicating a degeneracy between the $|\uparrow\rangle$ and $|S\rangle$ states. The full phenomenology explained above is qualitatively reproduced by a self-consistent Hartree-Fock treatment of a N-QD-S Anderson model (see Suppl. Information), thus supporting our interpretation in terms of spin-resolved Andreev levels and a QPT.
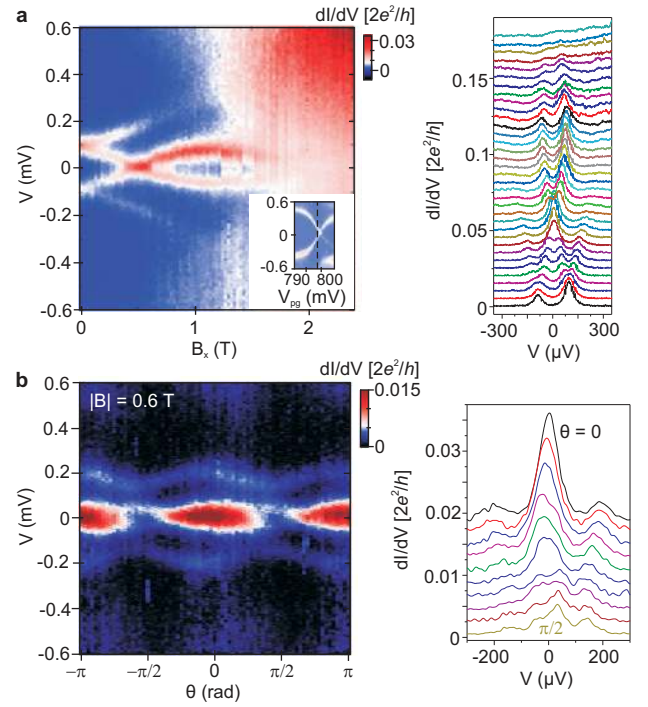

FIG. 4. **Magnetic-field induced QPT and angle anisotropy.** (a) Left panel: $dI/dV(B, V)$ taken at the position of the vertical line in the inset (same device as in Fig. 3). Right panel: line traces at equally spaced B values as extracted from the data in the left panel (each shifted by 0.005 $\times 2e^2/h$). The QPT induced by the field is observed as a ZBP extending over a B range of about 150 mT. This apparently large extension is a consequence of the finite width of the Andreev levels. (b) $dI/dV(V)$ traces taken with $|B| = 0.6$ T, at different angles. This field magnitude corresponds to the QPT field when B is aligned to the NW axis at $\theta = 0$ Owing to the g-factor anisotropy, the ZBP associated with the QPT is split and suppressed when B is rotated away from the NW axis. The peak splitting has a maximum at $\theta = \pi/2$

Interestingly, the splitting of Andreev levels appears to be gate dependent. It tends to vanish when the system is pushed deep into the singlet GS, and it is maximal near the phase boundaries. To further investigate this behaviour, we have measured $dI/dV(B, V)$ for fixed values of V_{pg}. These measurements were carried out on a second similar device (see Suppl. Information). The mid-panel of Fig. 3b displays the B_x dependence of the sub-gap resonances measured at position 1 in Fig. 3a. Initially, the energy of the Andreev levels increases, as expected for a doublet GS (see left panel). From a linear fit of the low-field regime, i.e. $\zeta(B_x) = \zeta(0) + E_Z/2$, where $E_Z = |g_x|\mu_B B_x$ is the Zeeman energy and μ_B is the Bohr magneton, we obtain a g-factor $|g_x| \approx 5.6$. For $B_x > 0.7$ T, the field-induced closing of the gap bends the Andreev levels down to zero-energy. Finally, above the critical field, a split Kondo resonance is observed, from which $|g_x| \approx 5.5$ is estimated, consistent with the value extracted from the Andreev level evolution. The mid-

panel of Fig. 3c displays a similar measurement taken at position 2 in Fig. 3a, where the GS is a singlet. The splitting of the Andreev levels is clearly asymmetric. The lower level decreases to zero according to a linear dependence $\zeta_\uparrow(B_x) = \zeta(0) - E_Z/2$, with $|g_x| \approx 6.1$, which is close to the value measured in the normal state. The higher energy level, however, exhibits a much weaker field dependence. Both the non-linear field dependence for $B_x > 0.7$ T in Fig. 3b and the asymmetric splitting in Fig. 3c can be explained in terms of a level-repulsion effect between the Andreev levels and the continuum of quasiparticle states. This interpretation is corroborated by numerical and analytical modeling, as discussed in the Suppl. Information. In the right panel of Fig. 3c, the inner sub-gap resonances cross around 1.5 T, denoting a field-induced QPT where the GS fermion parity changes from even to odd. Above this field, however, they remain pinned as a zero-bias peak (ZBP) up to $B_c^x \approx 2$ T. This peculiar behavior can be attributed to the level-repulsion effect discussed above, in combination with the rapid shrinking of Δ with B_x.

In order to observe a clear B-induced QPT from a singlet to a spin-polarized GS, we reduced $\zeta(0)$ by tuning V_{pg} closer to the singlet-doublet crossing in Fig. 3a. The corresponding data are shown in Fig. 4a. Contrary to the case of Fig. 3c, the Andreev level splitting is rather symmetric, owing to the reduced importance of the level repulsion effect at energies far from Δ. The inner sub-gap resonances split again after the QPT, which occurs now at $B_x \approx 0.5$ T. As expected, the outer sub-gap resonances get simultaneously suppressed (left panel of Fig. 3c). The suppression is not complete though, suggesting a partial population of the $|S\rangle$ ES, possibly favored by thermal activation.

We note that the ZBP at the QPT appears to extend on a sizable field range $\Delta B_x \approx 150$ mT. This range is consistent with the Γ_N-dominated lifetime broadening of the Andreev levels, i.e. $|g_x|\mu_B\Delta B_x \approx$ peak width $\approx 50\mu$eV. In Fig. 4b we show how the ZBP depends on the in-plane B angle, θ, relative to the NW axis. As θ varies from 0 to $\pi/2$, the ZBP splits into two peaks with decreasing height. This angle dependence is an effect of the g-factor anisotropy. For $\theta = \pi/2$, we find a g-factor $|g_y| \approx 3$, i.e.

a factor of 2 smaller than for $\theta = 0$ (see Suppl. Information). As a result, the QPT only occurs at a higher field (see Suppl. Information, $B_{QPT}^y \approx 1$ T), and the split peaks correspond to $\zeta_\uparrow$ transitions on the singlet-GS side. Figure 4b shows also a pair of small outer peaks associated with the $\zeta_\downarrow$ transitions. Their oscillatory position is as well due to g-factor anisotropy.

Noteworthy, the B dependences discussed above mimic some of the signatures expected for Majorana fermions in hybrid devices [7, 8, 35–43]. A ZBP extending over a sizable B range is observed for $\theta = 0$, and it is suppressed for $\theta = \pi/2$, i.e. when B is presumably aligned to the Rashba spin-orbit field, B_{SO} [39, 40]. While in Fig. 4 the field extension of the ZBP is limited by the ratio between the Andreev-level linewidth and the g-factor, Fig. 3b shows a ZBP extending over a much larger B range. This stretching effect is linked to the field-induced suppression of Δ and the consequently enhanced level repulsion with the continuum of quasiparticle states. In larger QDs or extended nanowires, a similar level-repulsion effect may as well arise from other Andreev levels present inside the gap [35, 36, 38, 44].

A more detailed discussion of the relation between the results of this work and existing experiments on Majorana fermions is given in section VII of the Supplementary Information. Interestingly, a recent study has shown that zero-energy crossings of Andreev levels associated with a change in the ground state parity, similar to those presented here, adiabatically evolve towards zero-energy Majorana modes, upon increasing the nanowire length to the infinite-length limit [44]. This evolution might be experimentally investigated in semiconductor-nanowire systems by studying the B-evolution of Andreev levels in nanowires of increasing length. Along similar lines, recent proposals have discussed the possibility of a gedanken experiment investigating the short-to-long wire evolution in chains of magnetic impurities deposited on superconducting surfaces [45–49]. In such proposals, the Yu-Shiba-Rusinov bound states induced by the individual magnetic impurities (similar to the Andreev levels discussed here), evolve towards a band when the length of the chain increases and may ultimately lead to Majorana modes localized at the edges of the atom chain.

[1] Franceschi, S. D., Kouwenhoven, L. P., Schönenberger, C. & Wernsdorfer, W. Hybrid superconductor-quantum dot devices. *Nature Nanotech.* **5**, 703–711 (2010).

[2] Hofstetter, L., Csonka, S., Nygård, J. & Schönenberger, C. Cooper pair splitter realized in a two-quantum-dot Y-junction. *Nature* **461**, 960–963 (2009).

[3] Herrmann, L. G. *et al.* Carbon nanotubes as Cooper pair splitters. *Phys. Rev. Lett.* **104**, 026801 (2010).

[4] Das, A. *et al.* High-efficiency Cooper pair splitting demonstrated by two-particle conductance resonance and positive noise cross-correlation. *Nature Commun.* **3**, 1165 (2012).

[5] Cleuziou, J., Wernsdorfer, W., Bouchiat, V., Ondarcuhu, T. & Monthioux, M. Carbon nanotube superconduct-

ing quantum interference device. *Nature Nanotech.* **1**, 53 (2006).

[6] Sau, J. D., Lutchyn, R. M., Tewari, S. & Sarma, S. D. Generic new platform for topological quantum computation using semiconductor heterostructures. *Phys. Rev. Lett.* **104**, 040502 (2010).

[7] Lutchyn, R. M., Sau, J. D. & Sarma, S. D. Majorana fermions and a topological phase transition in a semiconductor-superconductor. *Phys. Rev. Lett.* **105**, 077001 (2010).

[8] Oreg, Y., Refael, G. & von Oppen, F. Helical liquids and Majorana bound states in quantum wires. *Phys. Rev. Lett.* **105**, 177002 (2010).

[9] van Dam, J. A., Nazarov, Y. V., Bakkers, E. P. A. M.,

Franceschi, S. D. & Kouwenhoven, L. P. Supercurrent reversal in quantum dots. *Nature* **442**, 667–670 (2006).

[10] Buitelaar, M. R., Nussbaumer, T. & Schönenberger, C. Quantum dot in the Kondo regime coupled to superconductors. *Phys. Rev. Lett.* **89**, 256801 (2002).

[11] Jorgensen, H. I., Novotny, T., Grove-Rasmussen, K., Flensberg, K. & Lindelof, P. E. Critical current 0-π transition in designed Josephson quantum dot junctions. *Nano Lett.* **7**, 2441–2445 (2007).

[12] Maurand, R. *et al.* First-order 0-π quantum phase transition in the Kondo regime of a superconducting carbon nanotube quantum dot. *Phys. Rev. X* **2**, 011009 (2012).

[13] Doh, Y. J., Franceschi, S. D., Bakkers, E. P. A. M. & Kouwenhoven, L. P. Andreev reflection versus Coulomb blockade in hybrid semiconductor nanowire devices. *Nano Lett.* **8**, 4098–4102 (2008).

[14] Yamada, Y., Tanaka, Y. & Kawakami, N. Interplay of Kondo and superconducting correlations in the nonequilibrium andreev transport through a quantum dot. *Phys. Rev. B* **84**, 075484 (2011).

[15] Glazman, L. I. & Matveev, K. Resonant Josephson current through Kondo impurities in a tunnel barrier. *JETP Lett.* **49**, 659 (1989).

[16] Rozhkov, A. V. & Arovas, D. P. Josephson coupling through a magnetic impurity. *Phys. Rev. Lett.* **82**, 2788–2791 (1999).

[17] Vecino, E., Martín-Rodero, A. & Yeyati, A. L. Josephson current through a correlated quantum level: Andreev states and π junction behavior. *Phys. Rev. B* **68**, 035105 (2003).

[18] Oguri, A., Tanaka, Y. & Hewson, A. C. Quantum phase transition in a minimal model for the Kondo effect in a Josephson junction. *J. Phys. Soc. Japan* **73**, 2494 (2004).

[19] Bauer, J., Oguri, A. & Hewson, A. C. Spectral properties of locally correlated electrons in a Bardeen-Cooper-Schrieffer superconductor. *J. Phys.: Condens. Matter* **19**, 486211 (2007).

[20] Choi, M. S., Lee, M., Kang, K. & Belzig, W. Kondo effect and Josephson current through a quantum dot between two superconductors. *Phys. Rev. B* **70**, 020502(R) (2004).

[21] Meng, T., Florens, S. & Simon, P. Self-consistent description of Andreev bound states in Josephson quantum dot devices. *Phys. Rev. B* **79**, 224521 (2009).

[22] Domański, T., Donabidowicz, A. & Wysokiński, K. I. Meservey-Tedrow-Fulde effect in a quantum dot embedded between metallic and superconducting electrodes. *Phys. Rev. B* **78**, 144515 (2008).

[23] Futterer, D., Swieboddzinski, J., Governale, M. & König, J. Renormalization effects in interacting quantum dots coupled to superconducting leads. *Phys. Rev. B* **87**, 014509 (2013).

[24] Kanai, Y. *et al.* Electrical control of Kondo effect and superconducting transport in a side-gated InAs quantum dot Josephson junction. *Phys. Rev. B* **82**, 054512 (2010).

[25] Sand-Jespersen, T. *et al.* Kondo-enhanced Andreev tunneling in InAs nanowire quantum dots. *Phys. Rev. Lett.* **99**, 126603 (2007).

[26] Eichler, A. *et al.* Even-odd effect in Andreev transport through a carbon nanotube quantum dot. *Phys. Rev. Lett.* **99**, 126602 (2007).

[27] Pillet, J. D. *et al.* Andreev bound states in supercurrent-carrying carbon nanotubes revealed. *Nature Phys.* **6**, 965–969 (2010).

[28] Deacon, R. S. *et al.* Tunneling spectroscopy of Andreev energy levels in a quantum dot coupled to a superconductor. *Phys. Rev. Lett.* **104**, 076805 (2010).

[29] Dirks, T. *et al.* Transport through Andreev bound states in a graphene quantum dot. *Nature Phys.* **7**, 386–390 (2011).

[30] Lee, E. J. H. *et al.* Zero-bias anomaly in a nanowire quantum dot coupled to superconductors. *Phys. Rev. Lett.* **109**, 186802 (2012).

[31] Chang, W., Manucharyan, V. E., Jespersen, T. S., Nygård, J. & Marcus, C. M. Tunneling spectroscopy of quasiparticle bound states in a spinful Josephson junction. *Phys. Rev. Lett.* **110**, 217005 (2013).

[32] Pillet, J. D., Joyez, P., Zitko, R. & Goffman, M. F. Tunneling spectroscopy of a single quantum dot coupled to a superconductor: From Kondo ridge to Andreev bound states. *Phys. Rev. B* **88**, 045101 (2013).

[33] Kumar, A. *et al.* Temperature dependence of Andreev spectra in a superconducting carbon nanotube quantum dot. *arXiv:1308.1020v1* (2013).

[34] Giazotto, F. *et al.* A Josephson quantum electron pump. *Nature Phys.* **7**, 857–861 (2011).

[35] Prada, E., San-Jose, P. & Aguado, R. Transport spectroscopy of N-S nanowire junctions with Majorana fermions. *Phys. Rev. B* **86**, 180503(R) (2012).

[36] Rainis, D., Klinovaja, J. & Loss, D. Towards a realistic transport modeling in a superconducting nanowire with Majorana fermions. *Phys. Rev. B* **87**, 024515 (2013).

[37] Sarma, S. D., Sau, J. D. & Stanescu, T. D. Splitting of the zero-bias conductance peak as smoking gun evidence for the existence of the Majorana mode in a superconductor-semiconductor nanowire. *Phys. Rev. B* **86**, 220506(R) (2012).

[38] Liu, J., Potter, A. C., Law, K. T. & Lee, P. A. Zero-bias peaks in the tunneling conductance of spin-orbit-coupled superconducting wires with and without Majorana end-states. *Phys. Rev. Lett.* **109**, 267002 (2012).

[39] Mourik, V. *et al.* Signatures of Majorana fermions in hybrid superconductor-semiconductor nanowire devices. *Science* **336**, 1003–1007 (2012).

[40] Das, A. *et al.* Zero-bias peaks and splitting in an Al-InAs nanowire topological superconductor as a signature of Majorana fermions. *Nature Phys.* **8**, 887–895 (2012).

[41] Deng, M. T. *et al.* Anomalous zero-bias conductance peak in a Nb-InSb nanowire-Nb hybrid device. *Nano Lett.* **12**, 6414–6419 (2012).

[42] Finck, A. D. K., van Harlingen, D. J., Mohseni, P. K., Jung, K. & Li, X. Anomalous modulation of a zero-bias peak in a hybrid nanowire-superconductor device. *Phys. Rev. Lett.* **110**, 126406 (2012).

[43] Churchill, H. O. H. *et al.* Superconductor-nanowire devices from tunelling to multi-channel regime: zero-bias oscillations and magnetoconductance crossover. *Phys. Rev. B* **87**, 242401(R) (2013).

[44] Stanescu, T. D., Lutchyn, R. M. & Sarma, S. D. Dimensional crossover in spin-orbit-coupled semiconductor nanowires with induced superconducting pairing. *Phys. Rev. B* **87**, 094518 (2013).

[45] Nadj-Perge, S., Drozdov, I. K., Bernevig, B. A. & Yazdani, A. Proposal for realizing majorana fermions in chains of magnetic atoms on a superconductor. *Phys. Rev. B* **88**, 020407(R) (2013).

[46] Klinovaja, J., Stano, P., Yazdani, A. & Loss, D. Topological superconductivity and Majorana fermions in RKKY systems. *arXiv:1307.1442* (2013).

[47] Vazifeh, M. M. & Franz, M. Self-organized topolog-

ical state with Majorana fermions. *arXiv:1307.2279v1* (2013).

[48] Braunecker, B. & Simon, P. Interplay between classical magnetic moments and superconductivity in quantum one-dimensional conductors: Towards a self-sustained topological Majorana phase. *Phys. Rev. Lett.* **111**, 147202 (2013).

[49] Pientka, F., Glazman, L. & von Oppen, F. Topological superconducting phase in helical Shiba chains. *Phys. Rev. B* **88**, 155420 (2013).

[50] Jiang, X., Xiong, Q., Qian, F., Li, Y. & Lieber, C. M. InAs/InP radial nanowire heterostructures as high electron mobility devices. *Nano Lett.* **7**, 3214–3218 (2007).

Methods

Device fabrication. The N-QD-S devices used in this study were based on individual InAs/InP core/shell nanowires grown by thermal evaporation [50] (diameter ≈ 30 nm, shell thickness ≈ 2 nm). The NWs were deposited onto Si/SiO$_2$ substrates on which arrays of thin metallic striplines [Ti(2.5 nm)/Au(15 nm), width ≈ 50 nm] covered by a 8 nm-thick atomic layer deposition (ALD) HfO$_2$ film had been previously processed. During the measurements, the degenerately-doped Si substrate was used as a global backgate, whereas the striplines were used as local gates. Normal metal [Ti(2.5 nm)/Au(50 nm)] and superconductor [Ti(2.5 nm)/V(45 nm)/Al(5 nm)] leads were incorporated to the devices by means of standard e-beam lithography techniques (lateral separation ≈ 200 nm).

Author contributions

E.J.H.L. and S.D.F. conceived the experiment. X.J. grew the semiconductor nanowires under C.M.L.'s supervision. E.J.H.L. fabricated the devices and performed all the measurements under S.D.F's supervision. R.A. performed the Hartree-Fock calculations, and M.H. carried out the analytical study of the level-repulsion effect. E.J.H.L., S.D.F., R.A. and M.H. analysed and interpreted the results. All authors co-wrote the manuscript.

Additional information

Supplementary information accompanies this paper at www.nature.com/naturenanotechnology. Reprints and permissions is available online at http://npg.nature.com/reprintsandpermissions/. Correspondence and requests for materials should be addressed to S.D.F.